Chemical Geology, 99 (1992) 29–50
Elsevier Science Publishers B.V., Amsterdam

Gold deposition by sulfidation of ferrous Fe in the lacustrine sediments of the Pueblo Viejo district (Dominican Republic): The effect of Fe–C–S diagenesis on later hydrothermal mineralization in a maar–diatreme complex

Richard M. Kettler[a], Robert O. Rye[b], Stephen E. Kesler[c], Philip A. Meyers[c], José Polanco[d] and Norman Russell[d,α]

[a]*Department of Geology, University of Nebraska, Lincoln, NE 68588-0340, USA*
[b]*U.S. Geological Survey, MS 963, Denver, CO 80225, USA*
[c]*Department of Geological Sciences, University of Michigan, Ann Arbor, MI 48109-1063, USA*
[d]*Rosario Dominicana S.A., Apartado Postal 944, Santo Domingo, Dominican Republic*

(Received June 27, 1991; revised and accepted November 29, 1991)

ABSTRACT

Kettler, R.M., Rye, R.O., Kesler, S.E., Meyers, P.A., Polanco, J. and Russell, N., 1992. Gold deposition by sulfidation of ferrous Fe in the lacustrine sediments of the Pueblo Viejo district (Dominican Republic): The effect of Fe–C–S diagenesis on later hydrothermal mineralization in a maar–diatreme complex. In: P.A. Meyers, L.M. Pratt and B. Nagy (Guest-Editors), Geochemistry of Metalliferous Black Shales. Chem. Geol., 99: 29–50.

The Pueblo Viejo district, located in the Cordillera Central of the Dominican Republic, contains large Au–Ag deposits associated with acid-sulfate alteration within spilites, conglomerates and carbonaceous sedimentary rocks that were deposited in a maar–diatreme complex. Much of the Au mineralization occurs in pyritic, carbonaceous siltstones of the Pueblo Viejo Maar–Diatreme Member of the Cretaceous Los Ranchos Formation. Pyrite is the only Fe-bearing phase in mineralized rock, whereas siderite is the dominant Fe-bearing phase in siltstones distal to mineralization. Disseminated pyrite occurs as framboids, cubes, pyritohedra, concretions and cement. Early framboids occur throughout the district. Au occurs as inclusions in later non-framboid disseminated pyrite (NFDP); an occurrence that is interpreted to be indicative of contemporaneous deposition. Pyrite framboids exhibit a wide range of $\delta^{34}S_{CDT}$-values (-17.5 to $+4.8$‰) and are interpreted to have formed during biogenic reduction of pore-water sulfate. The NFDP yield restricted $\delta^{34}S_{CDT}$-values ($\bar{x}=-5.2$‰, $s=\pm 2.4$‰, $n=43$) similar to those obtained from later vein pyrite ($\bar{x}=-6.4$‰, $s=\pm 1.5$‰, $n=12$). Alunite and barite have $\delta^{34}S$-values ranging from $+18.8$ to $+21.6$‰. The interpretation that the NFDP, vein pyrite, alunite and barite, and possibly even the framboidal pyrite share a common source of igneous sulfur is supported by the $\delta^{34}S$ data. Siderite occurs as concretions and cement, contains abundant Mg ($Fe_{0.75}Mg_{0.19}Mn_{0.03}Ca_{0.02}CO_3$) and has $\delta^{13}C_{PDB}$- and $\delta^{18}O_{SMOW}$-values ranging from -2.5 to $+1.1$‰ and $+14.6$ to $+19.5$‰, respectively. These data are consistent with the interpretation that the siderite formed in lacustrine sediments and that the carbonate in the siderite is probably methanogenic, although contributions from oxidation of organic matter during biogenic sulfate reduction, thermal decarboxylation of organic matter, or magmatic vapor cannot be ruled out.

Disseminated Au mineralization in the sedimentary rocks formed when a hydrothermal fluid encountered reactive Fe^{2+} in diagenetic siderite. The ensuing pyrite deposition consumed H_2S and destabilized the $Au(HS)_2^-$ complex, leading to precipitation of Au. The capacity of the sedimentary rocks to consume H_2S and precipitate Au was controlled by the amount of non-pyrite Fe present as siderite. The abundance of siderite was controlled by the extent of pyrite formation during diagenesis.

Correspondence to: R.M. Kettler, Department of Geology, University of Nebraska, Lincoln, NE 68588-0340, USA.
[α]*Present address:* American–Pacific Honduras, Apartado Postal 342, San Pedro Sula, Honduras.

1. Introduction

In this paper we document the relation between sulfidation of ferrous Fe and disseminated Au mineralization in the carbonaceous sedimentary rocks of the Pueblo Viejo district and show that the distribution of reactive ferrous Fe was controlled by earlier Fe–C–S diagenesis. The Pueblo Viejo district is a large Au–Ag district in which the mineralization is associated with acid-sulfate alteration (Kesler et al., 1981; Russell et al., 1986; Muntean et al., 1990). There are two different types of mineralization at Pueblo Viejo: (1) early disseminated precious-metal mineralization (addressed in this paper); and (2) later vein-hosted base and precious-metal mineralization (Muntean et al., 1990). Approximately 60% of the gold in the Monte Negro orebody at Pueblo Viejo occurs as disseminated mineralization, and this disseminated mineralization makes the Pueblo Viejo deposits amenable to bulk mining methods (Muntean et al., 1990). Most of the disseminated mineralization, particularly in the Moore orebody, overprints carbonaceous sedimentary rocks that have been altered diagenetically (Kesler et al., 1981; Muntean et al., 1990; Russell and Kesler, 1991).

Experimental studies have established the importance of S as a Au-complexing ligand (Seward,1973; Wood et al., 1987; Shenberger and Barnes, 1989), and analyses of fluid inclusion gases have confirmed the presence of abundant H_2S in auriferous solutions (Norman, 1987; Hofstra et al., 1988). Gold deposition from such solutions can be effected by processes that reduce the activity of reduced S species, including oxidation (Seward, 1973; Hofstra et al., 1988; Shenberger and Barnes, 1989), boiling (perhaps with concomitant deposition of base-metal sulfides) (Drummond and Ohmoto, 1985; Reed and Spycher, 1985) or sulfidation of ferrous Fe (Phillips and Groves, 1983; Phillips et al., 1984; Böhlke, 1988; Hofstra et al., 1991). The importance of sulfidation to Au precipitation depends on the reactivity of Fe in the rocks to H_2S. The interaction between rock and the H_2S in hydrothermal fluid would be far different if the Fe were

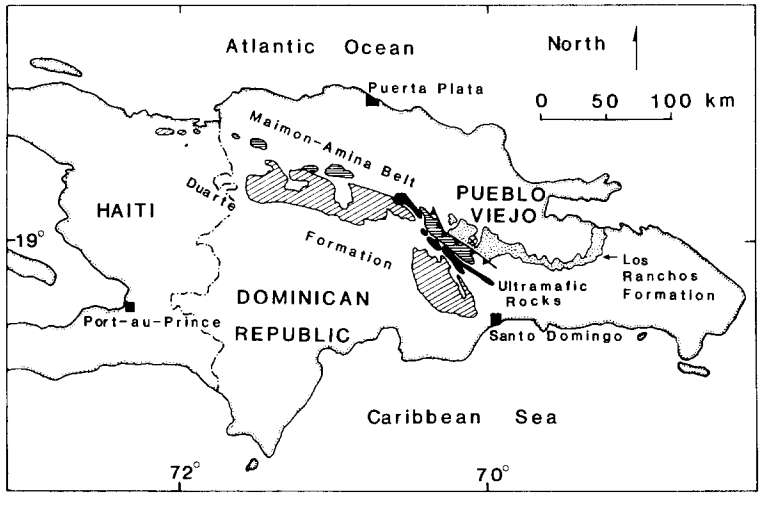

Fig. 1. Location of the Pueblo Viejo district in relation to the Duarte Formation, Maimon–Amina Belt and Los Ranchos Formation, Dominican Republic.

present as pyrite rather than as an oxide or carbonate.

In this paper we shall: (1) examine the mineralogy of disseminated precious-metal mineralization in the sedimentary rocks; (2) present geochemical evidence for district-wide sulfidation of ferrous Fe in siderite; (3) use $\delta^{34}S$-values of pyrite and ore-stage alunite and barite to identify the source of S in the hydrothermal system; (4) consider the efficacy of sulfidation as an ore-depositing mechanism; and (5) show that the distribution of diagenetic siderite and pyrite exerted a first-order control on later disseminated Au mineralization in the sedimentary rocks by controlling the availability of ferrous Fe for sulfidation by the hydrothermal fluids.

2. Geologic setting of the Pueblo Viejo district

The Pueblo Viejo district (Kesler et al., 1981, 1986; Russell et al., 1981, 1986; Muntean et al., 1990; Russell and Kesler, 1991) is located ~60 km northwest of Santo Domingo in the Cordillera Central, the axial mountain range on the island of Hispaniola (Fig. 1). The Cordillera Central consists largely of the actinolitic amphibolite of the Duarte Formation and of the albite–quartz–sericite schist of the Maimon–Amina Belt, which appear to represent oceanic crust and some of the earliest volcanic rocks in the Greater Antilles arc, respectively (Bowin, 1975). Mineralization at Pueblo Viejo is hosted by the Cretaceous Los Ranchos Formation (Kesler et al., 1981), which is ~125 Ma old; roughly the same age as the metamorphism of the Duarte and Maimon Formations (Bowin, 1975; Kesler et al., 1981).

The Los Ranchos Formation consists of spilite, keratophyre and clastic sedimentary rocks derived therefrom (Kesler et al., 1981, 1991; Russell and Kesler, 1991). The Pueblo Viejo Maar–Diatreme Member, which is the uppermost member in the Los Ranchos Formation, hosts mineralization in the Pueblo Viejo district (Fig. 2). The Pueblo Viejo Maar–Diatreme Member was deposited in a small sedimentary basin that has been interpreted to be a maar (Sillitoe and Bonham, 1984; Kesler et al., 1986) or maar–diatreme complex (Russell and Kesler, 1991). The base of the Pueblo Viejo Maar–Diatreme Member consists of breccias and lapilli ash tuffs considered to be coeval with diatreme formation (Russell and Kesler, 1991). The breccias are derived largely from the underlying spilite and volcaniclastic rocks of the Platanal Member (Kesler et al., 1991). The breccias and lapilli ash tuffs are overlain by spilite conglomerates that fine upward into interbedded spilite-derived arenites

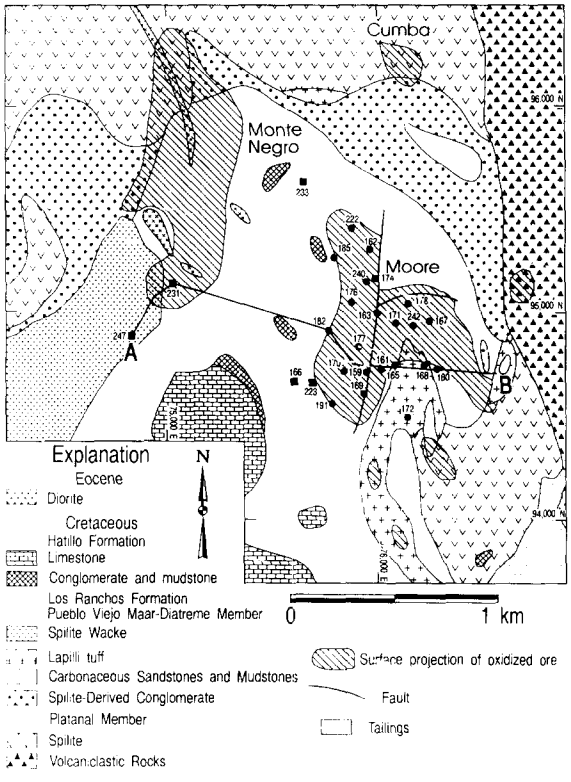

Fig. 2. Geological map of the Pueblo Viejo district after Russell and Kesler (1991). The *diagonal shading* marks the surface projection of the oxidized portions of the Moore, Monte Negro and Cumba orebodies. The *tick marks* match the grid lines shown in Fig. 9. *Squares* designate diamond drill holes that have intersected sideritic rocks. Other diamond drill holes referred to in the text and tables are shown as *circles*. The DDH prefix to the drill hole numbers that appears in the tables and text has been omitted from this figure.

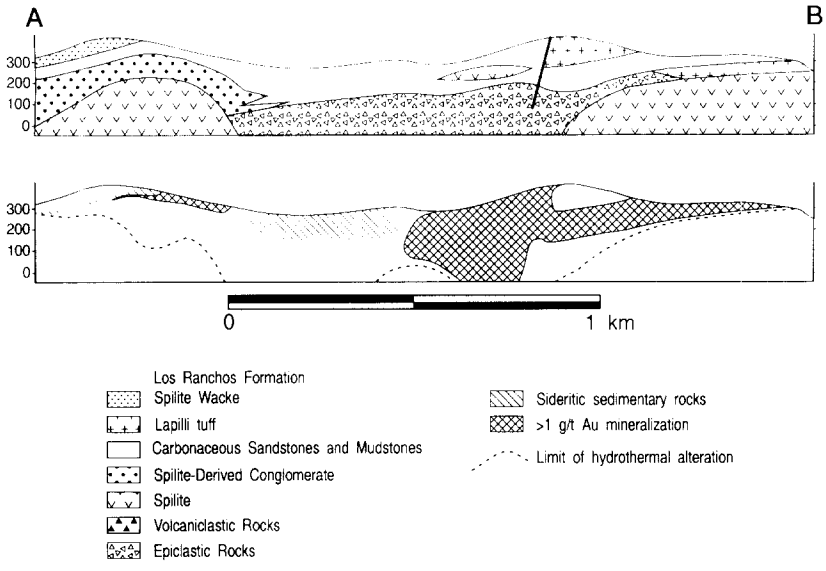

Fig. 3. Cross-section through the southern portions of the Moore and Monte Negro orebodies after Russell and Kesler (1991). Lower cross-section shows the distribution of Au mineralization and sideritic carbonaceous sedimentary rocks.

and finely laminated, black siltstones. These spilite-derived arenites and carbonaceous siltstones are referred to by Kesler et al. (1981) as the "carbonaceous sediments". Russell et al. (1986) and Russell and Kesler (1991) described abrupt lateral facies changes between conglomerates and the carbonaceous sedimentary rocks and suggested that the present west and northwest margins of the basin approximate its original boundaries. The extent of the basin to the south is unknown. The carbonaceous sedimentary rocks are dark-gray, thinly-laminated siltstones with interbedded medium-grained arenites that are as thick as 7 cm. The arenites exhibit sharp basal contacts and are graded locally. Load casts and lenticular bedding are widespread, and the arenites are locally cross-laminated. The siltstones are predominantly plane-laminated with local convolute bedding. Kesler et al. (1981) report local desiccation cracks and ripple marks. The unmineralized sedimentary rocks contain 1–2% total organic carbon. The organic matter occurs both as woody macerals in which cell walls are still visible in thin section and as amorphous organic matter localized along fractures (pyrobitumen) (Kettler et al., 1990). The carbonaceous sedimentary rocks contain abundant Fe, on average 6%, occurring as siderite or pyrite.

Siderite is present in the sedimentary rocks distal to mineralization whereas mineralized sedimentary rocks are pyritic and contain no siderite (Fig. 3). Locations of drill holes that have intersected siderite-bearing rocks are shown in Fig. 2. Siderite occurs as dark reddish-brown to orange-pink concretions that are as large as 1.5 cm in diameter, and as rims around wood fragments (Fig. 4). One bed or large concretion of siderite intersected by a diamond drill hole is 7 cm thick. Where bedding is discernible, it is deformed around the siderite concretions. In thin section the siderite occurs as an earthy, patchy cement and as concretions.

The two largest orebodies at Pueblo Viejo, Moore and Monte Negro, are located on the flanks of the sedimentary basin (Fig. 2). Mineralization comprises native Au, electrum and Au- and Ag-tellurides, with pyrite, sphalerite, enargite, and lesser bournonite, gratonite, chalcostibite, tennantite–tetrahedrite and boulangerite (Hartley and Wick, 1979; Kesler et al., 1981; Russell et al., 1986). Veins of py-

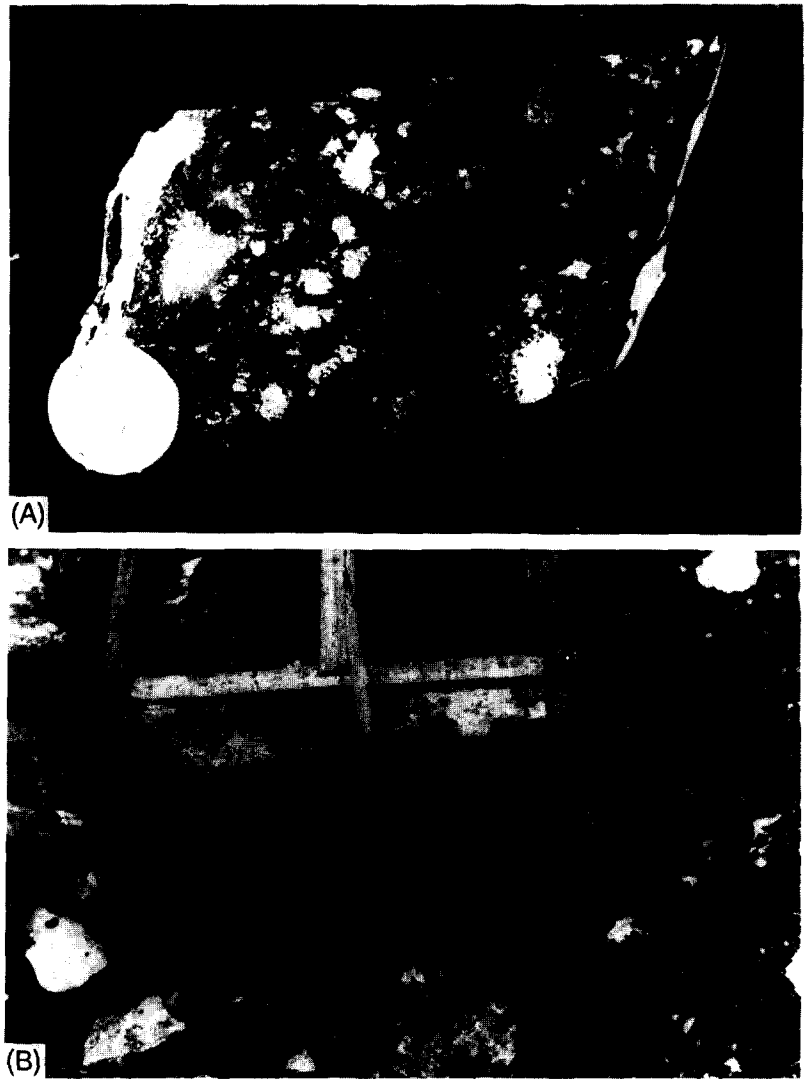

Fig. 4. A. Photo of siderite concretions in sample of carbonaceous sedimentary rock. Note *dime* for scale.
B. Photo of siderite rimming wood clast (in section of core on right). Note *pencil* for scale.

rite, enargite and sphalerite are abundant. The sulfides in these veins contain inclusions of sulfosalts, electrum and Au–Ag-tellurides. Muntean et al. (1990) have described the paragenesis of vein mineralization at Monte Negro. They note that barite occurs locally in the center of veins and as a coating on pyrite, indicating that it precipitated late in the paragenetic sequence. Traces of barite are also disseminated through mineralized carbonaceous sedimentary rocks. Alunite occurs in veins and is considered to be contemporaneous with much of the disseminated mineralization (Muntean et al., 1990). At shallow depths the sulfide mineralization has been oxidized by weathering and can be processed economically. Beneath the zone of weathering precious metals occur as inclusions in pyrite and cannot be extracted easily. Mapping of precious-metal contents indicates that the orebodies are funnel-shaped (Fig. 3; Kesler et al., 1981; Russell et al., 1986; Russell and Kesler, 1992). The throat of the funnel is located in spilite and spilite–clast conglomerates with the orebody

flaring out to a bowl-shaped geometry in the overlying carbonaceous sedimentary rocks. The age of Au mineralization is not known precisely. Although Au mineralization occurred after lithification of the maar sediments, it is believed to be related to hydrothermal processes that began prior to or contemporaneously with the formation of the maar (Russell and Kesler, 1992).

3. Analytical methods

Electron microprobe analyses of siderite were made on a Caméca® Camébax electron microprobe with an accelerating voltage of 15 kV, beam current of 10 nA and 5-μm beam diameter. Energy-dispersive spectra and backscattered electron images were monitored to insure that the electron beam sampled siderite only. Fe, Mg, Ca and Mn were determined using siderite, dolomite and rhodochrosite standards. Carbonate contents were calculated from stoichiometric relations.

Samples of siderite for stable carbon and oxygen isotopic analyses were obtained by drilling concretions with a 500-μm drill. The resulting powdered samples were heated at 200°C in vacuo for 1 hr to remove volatile contaminants. The samples were reacted with anhydrous phosphoric acid for 3 hr at 55°C. This is a relatively short reaction time and may result in incomplete yields. Siderite ground to 60 μm will yield 20% of the total CO_2 when reacted for 3 hr at 55°C (Rosenbaum and Sheppard, 1986). The sample produced by drilling consists of particles much smaller than 60 μm and should yield a much larger fraction of the total CO_2 (see Walters et al., 1972). Carpenter et al. (1988) reported that siderite prepared in this way had reacted completely within 20 min at 55°C. Incomplete reaction would not compromise the interpretation significantly. The CO_2 produced by partial reaction of calcite or dolomite is depleted in ^{18}O by less than 2‰ compared to CO_2 produced by complete reaction (Walters et al., 1972). The liberated CO_2 was processed in an on-line gas-extraction system linked to a VG® Micromass *602*E ratio mass spectrometer. The isotopic data obtained for siderite O were corrected for contribution of ^{17}O to the mass 44 beam (Craig, 1957) and for fractionation between CO_2 and phosphoric acid (Carothers et al., 1988). Analytical precision was better than ± 0.1‰ (1σ) monitored through daily analysis of NBS-*20*.

Samples of pyrite for $\delta^{34}S$ analyses were obtained by digesting the rock in concentrated hydrochloric acid for 24 hr followed by reaction with hydrofluoric acid for 1 week at room temperature. Spent hydrofluoric acid was decanted daily and fresh acid added. After dissolution of the silicate matrix was complete, the sample was rinsed to remove acid and panned to separate pyrite and kerogen. The pyrite separate was sieved and samples were hand-picked. Sulfur in pyrite was converted to SO_2 by heating with CuO at 1025°C for 10 min. Sulfur isotope analyses were made on a Nuclide *6-60*-RMS mass spectrometer with a modified source collector and pumping system. Analytical precision over the course of these analyses was determined to be ± 0.3‰ (1σ) as monitored by repeated analyses of NBS-*123*.

4. Disseminated mineralization

4.1. Disseminated pyrite

Pyrite is abundant in the carbonaceous sedimentary rocks in and adjacent to mineralization. It occurs as anhedral pyrite, framboids, pyritohedra, cubes, concretions and in lensoid masses (Kesler et al., 1981). Pyrite framboids occur in carbonaceous sedimentary rocks throughout the district as the earliest form of pyrite and are present in rocks that contain siderite. Framboids may occur singly or in polyframboidal aggregates. Age relationships among various forms of non-framboid dissem-

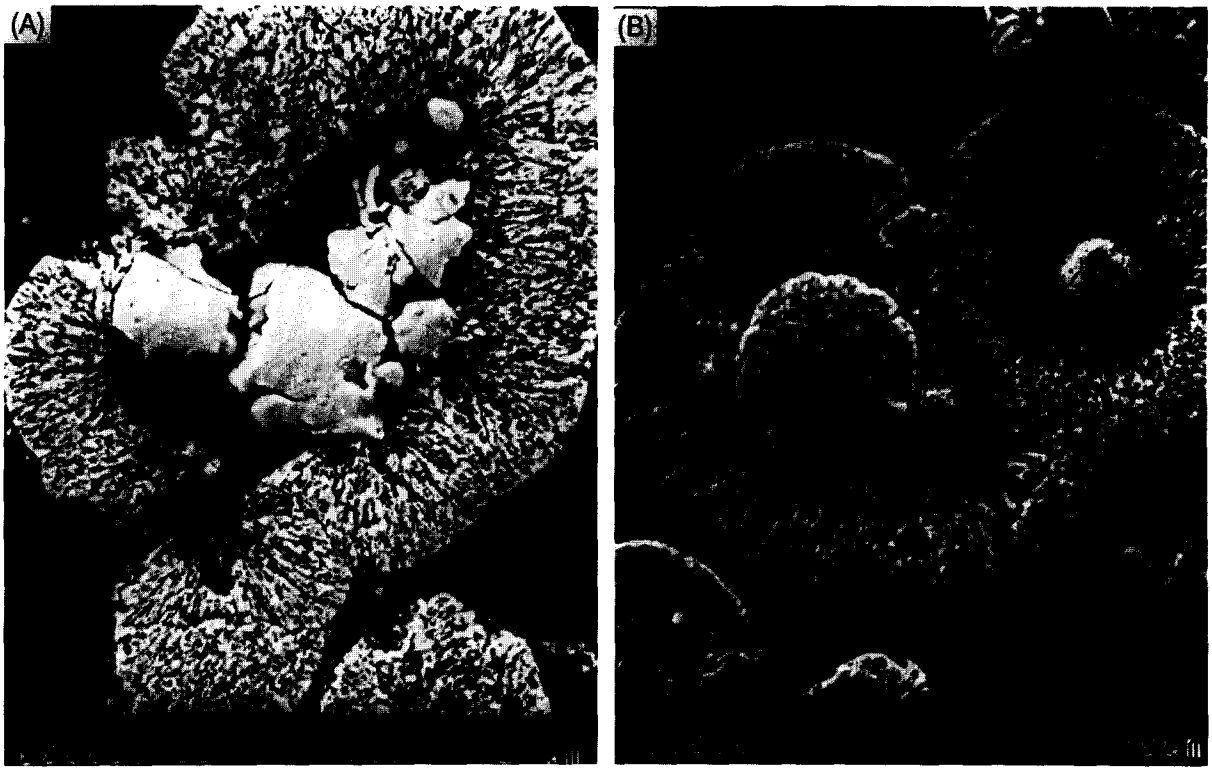

Fig. 5. A. Combination back-scattered and secondary electron image of radial pyrite rimming euhedral pyrite. B. Combination back-scattered and secondary electron image of radial pyrite rimming framboidal pyrite.

inated pyrite (NFDP) are unclear; various forms of pyrite may overgrow each other or anhedral pyrite.

Some pyrite exhibits radial textures (Fig. 5). Ramdohr (1980) interpreted such radial textures to be evidence of formation of pyrite from precursor marcasite. Kelly and Turneare (1970) document similar textures that they interpret to have formed during replacement of pyrrhotite by marcasite with subsequent replacement by pyrite. Radial pyrite is observed overgrowing both framboids and euhedral pyrite (Fig. 5), indicating that it post-dates formation of some euhedral pyrite. Fragments of all types of pyrite occur as inclusions in pyrite veins, indicating that veining occurred after deposition of much of the disseminated pyrite.

4.2. Disseminated base- and precious-metal mineralization

The most abundant sulfosalts in the disseminated mineral assemblage are gratonite and enargite. Both gratonite and enargite fill pore spaces in framboids and polyframboidal aggregates, and cement polyframboidal aggregates (Fig. 6). Sulfosalt deposition occurred after deposition of pyrite framboids.

Gold occurs predominantly as the native metal and as the Au-telluride calaverite. Both native Au and calaverite occur as inclusions within euhedral and anhedral pyrite (Fig. 7), indicating that the Au mineralization and Fe-sulfide deposition were linked geochemically. Calaverite is identified by its composition in

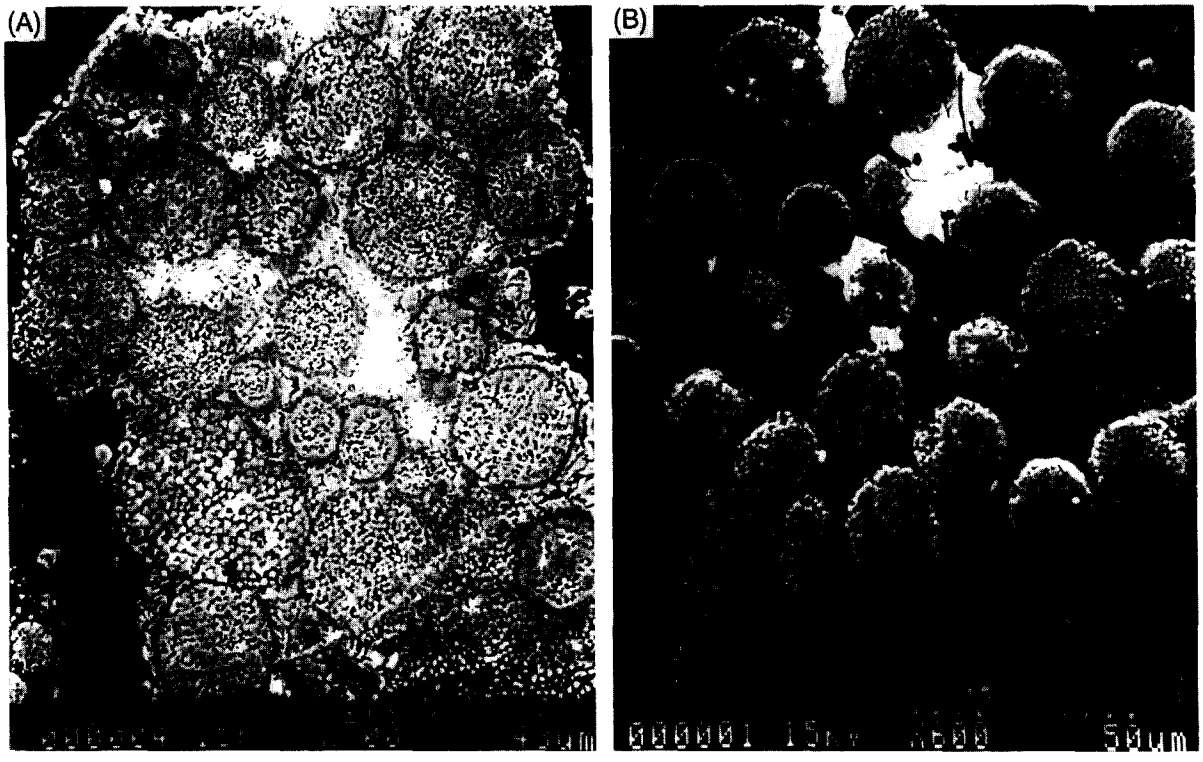

Fig. 6. A. Combination back-scattered and secondary electron image of gratonite filling pore spaces in a polyframboidal aggregate.
B. Combination back-scattered and secondary electron image of enargite cementing pyrite framboids together.

energy-dispersive spectrometric (EDS) analyses. In one case Au occurs as an inclusion in the pyrite that cements a polyframboidal aggregate. Au inclusions typically occur in pyrite grains that contain abundant microvoids (Fig. 7). Fig. 7A is an example of an anhedral mass of porous pyrite that has been overgrown by cubic pyrite. Similar microvoids have been observed in Bolivian Sn deposits (Kelly and Turneare, 1970) and massive sulfide deposits (Rye et al., 1984). Kelly and Turneare (1970) interpret the microvoids as resulting from replacement of pyrrhotite by pyrite under S-deficient conditions. Under these conditions the change in volume is negative and porosity develops in the pyrite. The same reasoning could be applied to most possible FeS precursors to pyrite. Electrum, which is moderately abundant in samples of vein pyrite, has not been observed in wallrock. Ag does occur in Cu–Ag-telluride phases that occur as inclusions within pyrite.

4.3. Pyrite morphology

Pyrite morphology varies with degree of precious-metal mineralization. Anhedral pyrite predominates in samples collected from the ore zone while in poorly mineralized and unmineralized rocks euhedral pyrite predominates. To quantify these observations, grain counts were performed on 39 samples that were representative of all lithologies and that were distributed through the Moore orebody (Fig. 2). The grain counts were made by traversing a polished section and counting all grains that could be resolved in a 0.5-mm field of view. Each pyrite grain was classified as a framboid, euhedral pyrite or anhedral pyrite (Table 1). Because data were collected from spilite as well as sedimentary rocks, the results were normalized to a framboid-free basis. Although the samples were classified as being "mineralized" (Au content >1 ppm) or "unmineralized"

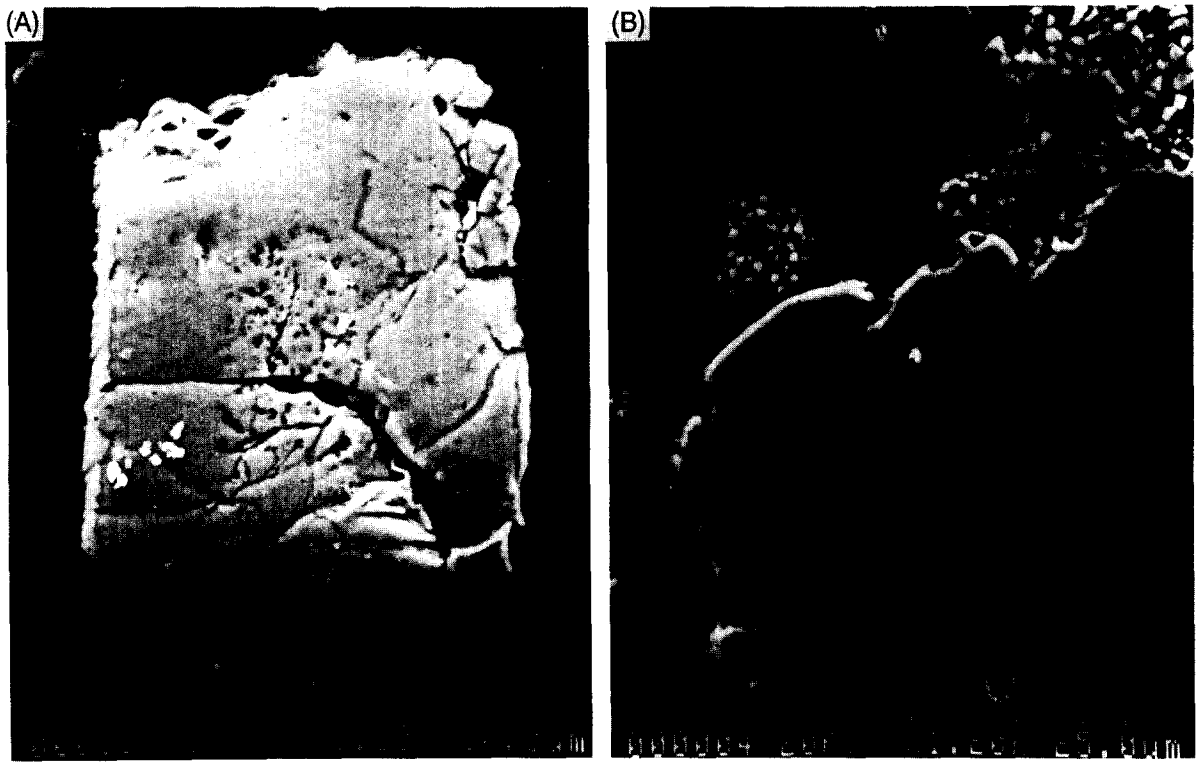

Fig. 7. A. Combination back-scattered and secondary electron image of Au inclusions in pyrite.
B. Combination back-scattered and secondary electron image of calaverite inclusion in pyrite.

(Au content < 1 ppm) it should be noted that all samples contain Au well in excess of average crustal abundances. The fraction of anhedral pyrite is greater in mineralized samples than in unmineralized samples (Fig. 8). Applying a two-sample Student's *t*-test allows one to reject the null hypothesis (that there is no difference in the fraction of anhedral pyrite in the mineralized and unmineralized populations) with an attained significance of < 0.005.

The anhedral pyrite may reflect the existence of an FeS precursor to some of the pyrite. Schoonen and Barnes (1988) have shown that pyrite does not nucleate in experimental systems that are supersaturated with respect to pyrite, but forms by replacement of an FeS precursor. If this precursor typically did not form euhdral crystals or was amorphous then the anhedral pyrite would reflect the nucleation of the precursor FeS during mineralization. In experiments to evaluate the importance of fluid chemistry on pyrite morphology, Murowchick and Barnes (1987) noted the occurrence of a fine-grained sulfide lacking any distinctive morphology. They considered the fine-grained sulfide to have resulted from the saturation of another Fe-sulfide phase with consequent precipitation of that phase.

The association of anhedral pyrite with disseminated Au mineralization and euhedral pyrite with barren rock has also been noted in the disseminated, pyritic Au orebodies at Alleghany, California, U.S.A. (J.K. Böhlke, pers. commun., 1990). The relation between ore grade and disseminated pyrite morphology indicates that much of the disseminated Fe-sulfide precipitated during mineralization rather than during biogenic sulfate reduction.

TABLE 1

Results of pyrite grain counts

Specimen	Au content (ppm)	Anhedral pyrite (%)	Euhedral pyrite (%)	*n*
DDH-*174-60*	8.75	38	62	1,990
DDH-*176-30*	4.05	61	39	1,034
DDH-*167-101*	3.5	58	42	982
DDH-240-80.1	3.25	71	29	2,601
DDH-*177-170*	3.15	60	40	2,429
DDH-*163-62*	3.00	50	50	252
DDH-*180-56*	2.8	70	30	685
DDH-*171-90*	2.75	64	36	1,480
DDH-*178-63*	2.65	63	37	1,109
DDH-*242-134.8*	2.3	60	40	2,704
DDH-*163-40*	2.0	76	24	1,719
DDH-*170-110*	2.0	66	34	1,683
DDH-*165-150*	2.0	64	36	927
DDH-*161-85*	2.0	62	38	806
DDH-*176-180*	1.8	58	42	1,633
DDH-*185-115*	1.65	40	60	525
DDH-*159-152*	1.5	44	56	1,639
DDH-*240-23.5*	1.25	87	13	2,608
DDH-*161-48*	1.25	59	41	3,387
DDH-*169-70*	1.25	51	49	212
DDH-*166-216*	0.75	25	75	1,223
DDH-*168-240*	0.75	22	78	1,295
DDH-*180-166*	0.5	41	59	1,480
DDH-*182-26*	0.45	21	79	520
DDH-*191-86.5*	0.3	43	57	860
DDH-*172-50*	0.25	37	63	1,164
DDH-*162-119*	0.0	91	9	787
DDH-*166-53*	0.0	63	37	1,070
DDH-*222-45.45*	0.0	56	44	1,499
DDH-*223-32.5*	0.0	52	48	1,139
DDH-*160-142*	0.0	52	48	926
DDH-*180-230*	0.0	51	49	545
DDH-*240-125*	0.0	48	52	926
DDH-*242-196.5*	0.0	44	56	2,486
DDH-*240-108*	0.0	42	58	1,232
DDH-*191-143*	0.0	39	61	390
DDH-*233-81.5*	0.0	38	62	2,480
DDH-*242-209.6*	0.0	36	64	622
DDH-*222-43.6*	0.0	30	70	807

n = number of grain counts.

5. District-scale evidence for sulfidation

The district-scale zoning of Au, siderite and pyrite (Figs. 2 and 3) suggests that S and Au were introduced together in carbonaceous sedimentary rocks. In order to map the effects of sulfidation of rocks at Pueblo Viejo, the degree

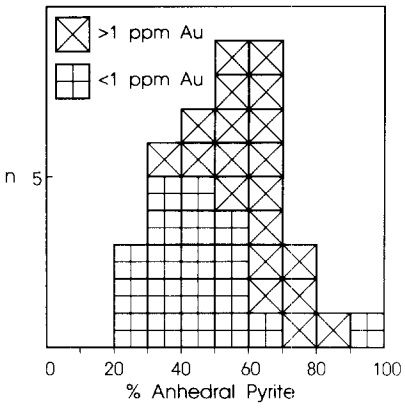

Fig. 8. Histogram of pyrite grain count data.

of sulfidation (DOS) was defined according to:

$$DOS = wt\%\ S / [(1.15)(wt\%\ Fe)] \quad (1)$$

[The acronym DOS has also been used by Boesen and Postma (1988) and Middelburg (1990). They define it differently.] The coefficient 1.15 is the Fe/S mass ratio in pyrite; thus, in the DOS notations, S contents are normalized to the amount of S necessary to convert all Fe in the rock to pyrite.

Fe and S assay data were used to calculate DOS over 2-m intervals. The DOS data were then averaged for an entire drill hole, plotted on a map and contoured (Fig. 9). The DOS data shown in Fig. 9 are not limited to the carbonaceous sedimentary rocks because all lithologies have been affected by sulfidation. Ferrous Fe in the carbonaceous sedimentary rocks occurs as siderite; whereas, chlorite, actinolite and magnetite occur in the spilite. When the DOS-values are compared for similarly averaged data for Au abundances (Fig. 9), significant overlap of the areas that contain ore-grade Au mineralization and high-DOS rock becomes apparent. The high values of DOS result from S addition and not from Fe depletion. In general, mineralized carbonaceous sedimentary rocks in the Moore orebody contain more Fe than is present in unmineralized carbonaceous sedimentary rocks (Kettler et al., 1987). Muntean et al. (1990) examined elemental gains and losses in spilite in the Monte

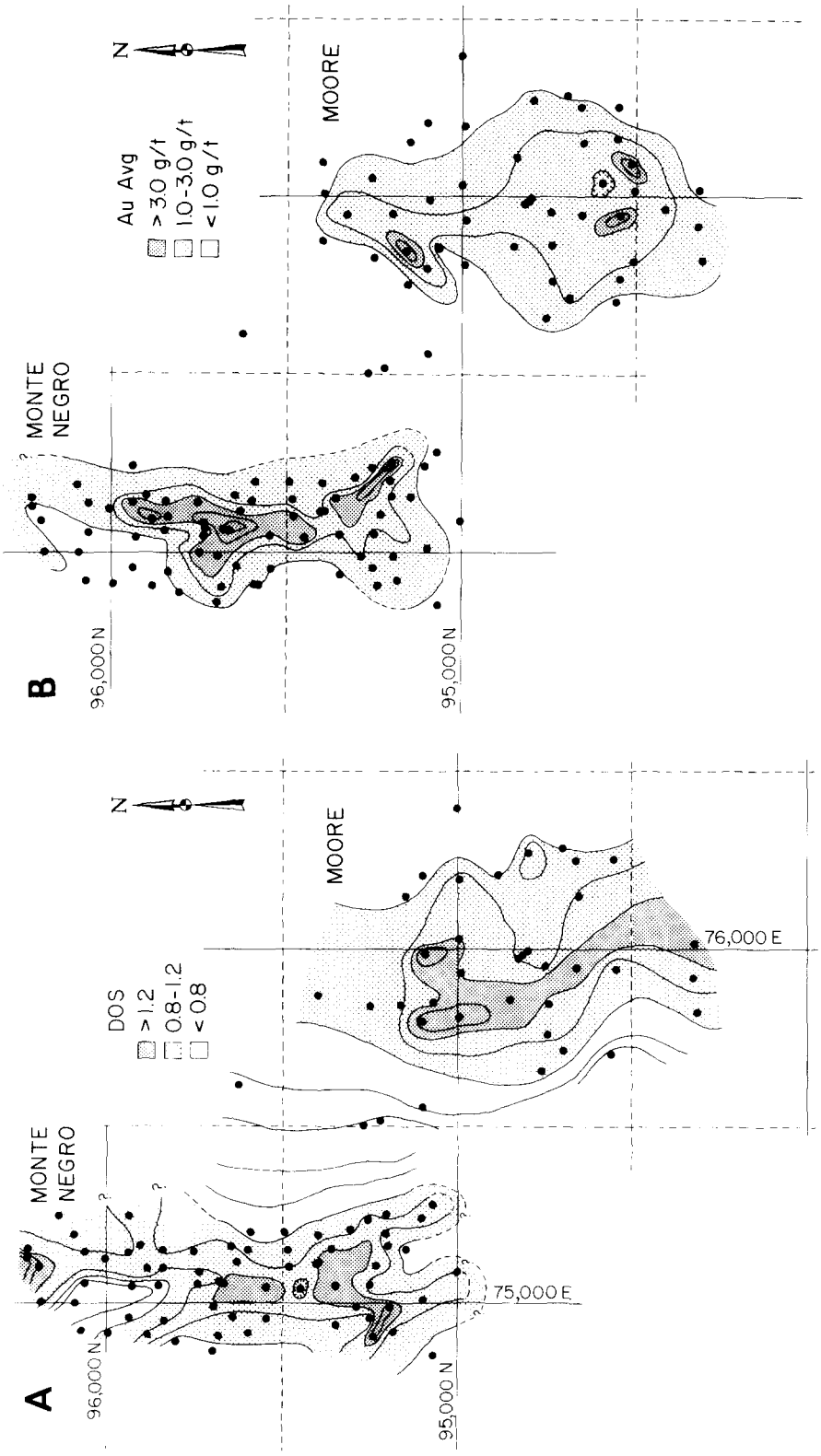

Fig. 9. A. Maps of the Moore and Monte Negro orebodies showing variation in the degree of sulfidation (DOS). *Solid grid lines* are 1 km apart. Grid lines correspond to tick marks shown in Fig. 2.
B. Maps of the Moore and Monte Negro orebodies showing variations in average Au grade. Scale is the same as for (A).

Negro orebody and were able to demonstrate that Fe was added to rocks during mineralization.

In the central portions of the Moore and Monte Negro orebodies, DOS-values exceed unity (Fig. 9), indicating that S is present in amounts exceeding those required for complete pyritization of Fe. Locally the S can be balanced by considering only sphalerite, enargite and barite. S is also accommodated in organic matter, which contains up to 14 wt% S (Kettler et al., 1990), in native S (Kesler et al., 1981), in alunite, and in a variety of sulfides and sulfosalts. Native S occurs both in veins (Kesler et al., 1981) and disseminated through the rock. Soxhlet extractions of 30-g samples of rock from the Moore orebody yielded small amounts (1–5 mg) of native S.

6. Elemental and isotopic chemistry of siderite

Siderite is a product of diagenesis in the carbonaceous sedimentary rocks, as indicated by its occurrence as concretions and cement, its association with organic matter (Fig. 4), and its restriction to the carbonaceous sedimentary rocks. Diagenetic or authigenic siderite forms in three settings: (1) methanic environments in which aqueous sulfate is depleted (Berner, 1981); (2) post-oxic environments by oxidation or thermal decarboxylation of organic matter (Berner, 1981); and (3) volcanic environments where CO_2 is introduced into crater lakes or maars from an underlying magma (Bernard and Symonds, 1989; Giggenbach, 1990).

Although the isotopic composition of siderite cannot be used to identify unique sources of CO_2 and H_2O from which the siderite precipitated, the elemental and isotopic chemistry of siderite can provide important insights into the chemistry of diagenetic fluids and the chemical environment in which the siderite was deposited. The $\delta^{13}C_{PDB}$-values of carbonate in the Pueblo Viejo siderites range from −2.5 to +1.1‰ (Table 2) and the $\delta^{18}O_{SMOW}$-values range from +14.6 to +19.5‰ (Table 2). Fig. 10 is a plot of the $\delta^{13}C$- and $\delta^{18}O$-values obtained from siderites at Pueblo Viejo compared with data compiled from the literature showing siderites of different origins. Many of the literature data shown were published before measurement of the siderite–phosphoric acid-liberated CO_2 fractionation factors (Rosenbaum and Sheppard, 1986; Carothers et al., 1988) and many of the authors have used calcite–acid-liberated CO_2 fractionation factors in order to determine the $\delta^{18}O$-values for siderite. The $\delta^{18}O$-values have been plotted as they were reported and are larger by 1–2‰ than those that would be obtained using the siderite–acid liberated CO_2 fractionation factors.

The Pueblo Viejo siderite has low $\delta^{18}O$-values indicating precipitation from solutions dominated by meteoric water. Siderites that

TABLE 2

Results of $\delta^{13}C$ and $\delta^{18}O$ analyses of siderite and $\delta^{13}C$ analyses of kerogen

Specimen	Substance	$\delta^{13}C_{PDB}$ (‰)	$\delta^{18}O_{SMOW}$ (‰)
DDH-*162-117-1*	siderite	−0.3	+16.7
DDH-*162-117-2*	siderite	−0.5	+15.2
DDH-*162-104-1*	siderite	−0.6	+14.6
DDH-*231-51-1*	siderite	−2.3	+15.1
DDH-*231-100-2*	siderite	−2.5	+15.7
DDH-*233-49.3-1*	siderite	+0.7	+15.1
DDH-*233-49.3-2*	siderite	+0.8	+14.9
DDH-*233-43.5-1*	siderite	+0.0	+17.8
DDH-*233-73.5-1*	siderite	+0.6	+17.4
DDH-*233-73.5-2*	siderite	+0.5	+16.5
DDH-*233-41.5A-1*	siderite	+0.1	+19.5
DDH-*233-41.5A-2*	siderite	+1.1	+16.7
DDH-*233-41.5A-3*	siderite	+1.0	+16.8
DDH-*223-46.5*	kerogen	−27.2	
DDH-*223-46.5*	kerogen	−27.3	
DDH-*233-41.5A*	kerogen	−31.7	
DDH-*233-41.5B*	kerogen	−30.6	
DDH-*233-72*	kerogen	−35.8	
DDH-*240-23.3*	kerogen	−26.9	
DDH-*240-23.5*	kerogen	−26.5	
DDH-*240-88.5*	kerogen	−25.4	
DDH-*240-95.5*	kerogen	−25.2	
DDH-*242-70.45B*	kerogen	−25.1	
DDH-*242-134.8*	kerogen	−24.9	
DDH-*242-209.6*	kerogen	−25.0	

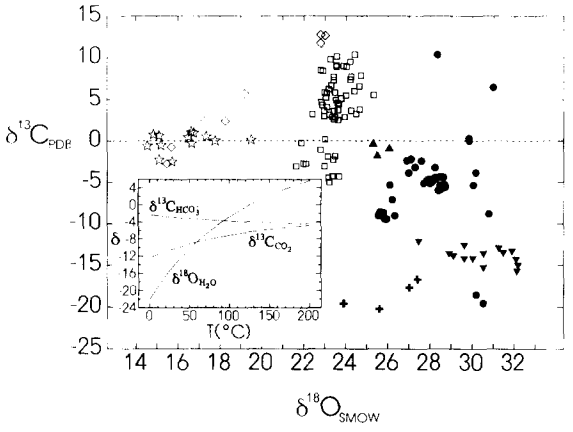

Fig. 10. Plot of the $\delta^{13}C$- and $\delta^{18}O$-values of siderite from Pueblo Viejo and other data reported from the literature. The *inset* shows the $\delta^{13}C$-values of CO_2 and HCO_3^- and $\delta^{18}O$-value of H_2O in equilibrium with siderite with an average $\delta^{13}C_{PDB} = -0.2‰$ and $\delta^{18}O_{SMOW} = +16.3‰$ (the average for the Pueblo Viejo data). Data from this study are designated by *open stars*, other data designated by *open symbols* are siderites that formed in non-marine sediments, whereas data designated by *filled symbols* are siderites that formed in marine sediments. All siderites plotted are classified as methanogenic or post-oxic using the data and interpretations as reported by the authors. □ = methanogenic siderite (Curtis et al., 1986); ◇ = methanogenic siderite (Fritz et al., 1971); ● = methanogenic siderite (Gautier, 1982); ▲ = methanogenic siderite (Maynard, 1982); + = post-oxic siderite (Maynard, 1982); ▼ = post-oxic siderite (Carpenter et al., 1988).

form in marine sediments typically have higher $\delta^{18}O$-values (Fig. 10). The $\delta^{18}O$-value of pore water in equilibrium with siderite could have ranged from ~ -22 to $\sim -3‰$ at temperatures ranging from 0° to 100°C, respectively (Fig. 10). The siderite could not have been in equilibrium with seawater, unless precipitation occurred at unreasonably high temperatures ($> \sim 20°C$).

We cannot identify a unique source of carbonate for the Pueblo Viejo siderite from the $\delta^{13}C$ data. Production of CO_2 by oxidation or decarboxylation of organic matter should yield siderite with low $\delta^{13}C$-values similar to that of the organic matter (-28 to $-33‰$, Table 2) (Irwin et al., 1977; Maynard, 1982), whereas CO_3^{2-} liberated to the fluid phase during

TABLE 3

Composition of siderite determined by electron microprobe

Specimen	X_{FeCO_3}	X_{MnCO_3}	X_{MgCO_3}	X_{CaCO_3}
DDH-*166-53-1*	0.74	0.05	0.20	0.01
DDH-*166-53-2*	0.72	0.04	0.22	0.01
DDH-*166-53-3*	0.75	0.04	0.20	0.01
DDH-*166-53-4*	0.77	0.04	0.18	0.01
DDH-*166-53-5*	0.75	0.04	0.19	0.01
DDH-*166-53-6*	0.76	0.04	0.19	0.01
DDH-*166-53-7*	0.76	0.04	0.19	0.01
DDH-*166-53-8*	0.73	0.04	0.22	0.01
DDH-*233-49.3-1*	0.71	0.02	0.22	0.04
DDH-*233-49.3-2*	0.76	0.02	0.20	0.02
DDH-*233-49.3-3*	0.76	0.02	0.20	0.01
DDH-*233-49.3-4*	0.72	0.03	0.22	0.03
DDH-*233-49.3-5*	0.72	0.02	0.22	0.03
DDH-*233-49.3-6*	0.74	0.02	0.21	0.03
DDH-*233-73.5-1*	0.81	0.02	0.14	0.03
DDH-*233-73.5-2*	0.80	0.02	0.13	0.04
DDH-*233-81.5-1*	0.81	0.02	0.12	0.04

methanogenesis contains much heavier C, with $\delta^{13}C$ approaching $+15‰$ (Irwin et al., 1977; Maynard, 1982; Curtis et al., 1986). Magmatically derived CO_2 has $\delta^{13}C$-values of -8 to $-5‰$ (Hoefs, 1980). Aqueous bicarbonate and CO_2 gas in equilibrium with the siderite would have had $\delta^{13}C$-values ranging from -12 to $-2‰$, respectively, at 0°C, to -7 and $-4‰$, respectively, at 100°C (Fig. 10). Although the $\delta^{13}C$ data are consistent with CO_2 contributions from all the above sources, our preferred interpretation is that the Pueblo Viejo siderite precipitated during methanogenesis. The occurrence of the siderite as concretions and cement that locally rim wood clasts (Fig. 4), its abundance in the carbonaceous sedimentary rocks and absence in other lithologies is strong evidence for a methanic or post-oxic origin. If the carbonate were derived predominantly from magmatic CO_2, siderite would have formed in all lithologies. The $\delta^{13}C$-values are more similar to siderites considered to have formed during methanogenesis than they are to siderites interpreted to have formed during post-oxic diagenesis (Fig. 10).

The elemental composition of siderite has

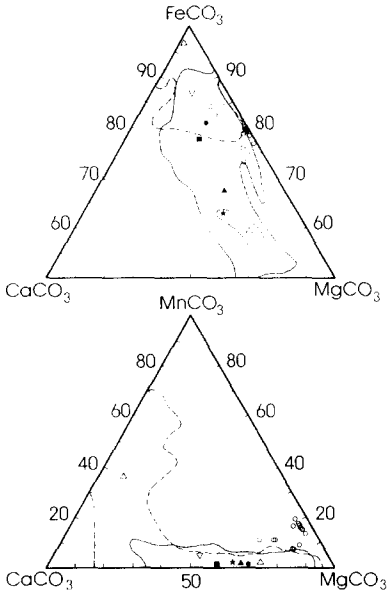

Fig. 11. Composition of Pueblo Viejo siderite (○) compared with compositions of siderite analyzed by Mozley (1989). The *dashed line* encloses the fields occupied by freshwater siderites whereas the *solid line* encloses the range of compositions for siderites that formed in marine sediments. Average values are denoted by the *symbols* and include: freshwater siderites from the Tyonek Formation (△) and the Ivishak Formation (▽); and marine siderites from the Ivishak Formation (●), Barrow Sandstone, Sag River and Shublik Formations (■), Kuparuk River Formation (▲) and Stevens Sandstone (★).

been used to identify a marine or freshwater origin for siderite. Matsumoto and Ijima (1981) and Mozley (1989) have shown that siderite deposited during diagenesis of freshwater sediments will have low Mg/Ca, Mg/Mn and Mg/Fe ratios. Electron microprobe analyses of the Pueblo Viejo siderite indicate that it is magnesian siderite (19 mole% $MgCO_3$) with high Mg/Ca and Mg/Fe ratios (Table 3; Fig. 11). However, the Pueblo Viejo siderites have lower Mg/Mn ratios than most marine siderites and higher Mg/Ca ratios than both non-marine and marine siderites. We interpret the elemental compositions of the Pueblo Viejo siderite to reflect precipitation of the siderite from lacustrine waters that have reacted extensively with spilites. Spilites in the Los Ranchos Formation contain abundant chlorite (Kesler et al., 1992) and are rich in Mg. Interaction of spilite-derived detritus with acidic, reduced waters would produce pore waters rich in Mg, Fe and Mn. A possible modern analog for these waters could be those in Lake Nyos, Cameroon. Lake Nyos is a maar containing water that is greatly enriched in Mg and Mn relative to most lacustrine waters, and is greatly enriched in Mn relative to seawater (Giggenbach, 1990).

7. Sulfur isotope data and the origin of disseminated pyrite

Sulfur isotope data were collected to determine the relation between disseminated pyrite and vein pyrite, to identify the source of sulfur in the pyrite at Pueblo Viejo and to make inferences regarding the factors that might limit pyrite formation during diagenesis. The latter role is particularly important because the abundant sulfide, sulfate and native S mineralization results in very high S/C ratios (Kesler et al., 1981) and values of the degree of pyritization (DOP). Although these parameters are used commonly in studies of diagenesis (e.g., Leventhal, 1983; Raiswell et al., 1988), the S content of these rocks is not controlled merely by diagenetic processes; the use of DOP or C/S plots to make inferences regarding the environment of deposition or diagenetic processes in this setting is inappropriate.

Each of the different morphologies of pyrite was sorted into hand-picked separates and analyzed for $\delta^{34}S$. Individual samples consisted of polyframboidal aggregates, cubes, pyritohedra, anhedral pyrite, concretions, monomineralic pyrite layers ("beds"), or samples of vein pyrite. The results of these analyses are presented in Table 4 and Fig. 12. Four observations summarize these data:

(1) Pyrite framboids exhibit the greatest spread in $\delta^{34}S$-values, ranging from -17.5 to $+4.8$‰.

(2) All other types of disseminated pyrite have $\delta^{34}S$-values that range from -11.8 to 0.0‰ with an average of -5.2‰.

TABLE 4

δ^{34}S-values of samples from the Pueblo Viejo district

Specimen	Orebody	Lithology	Sample	$\delta^{34}S_{CDT}$ (‰)	Source*
DDH-*240-87*	Moore	carbonaceous sedimentary rocks	anhedral pyrite	−4.7	[*1*]
DDH-*242-70.45*	Moore	carbonaceous sedimentary rocks	anhedral pyrite	−3.4	[*1*]
DDH-*242-134.8*	Moore	carbonaceous sedimentary rocks	anhedral pyrite	−4.7	[*1*]
DDH-*233-41.5*	Moore	carbonaceous sedimentary rocks	anhedral pyrite	−3.8	[*1*]
DDH-*195-248*	Monte Negro	spilite	anhedral pyrite	−6.1	[*1*]
DDH-*195-160*	Monte Negro	spilite	anhedral pyrite	−10.6	[*1*]
DDH-*195-250.5*	Monte Negro	spilite	anhedral pyrite	−9.0	[*1*]
DDH-*196-140*	Monte Negro	spilite	anhedral pyrite	−0.1	[*1*]
DDH-*240-23.5*	Moore	carbonaceous sedimentary rocks	pyrite concretion	−3.4	[*1*]
DDH-*240-95.5*	Moore	carbonaceous sedimentary rocks	pyrite concretion	−6.9	[*1*]
DDH-*240-98*	Moore	carbonaceous sedimentary rocks	pyrite concretion	−2.9	[*1*]
DDH-*240-102*	Moore	carbonaceous sedimentary rocks	pyrite concretion	−4.9	[*1*]
DDH-*233-41.5*	Moore	carbonaceous sedimentary rocks	pyrite concretion	−2.9	[*1*]
DDH-*233-72*	Moore	carbonaceous sedimentary rocks	pyrite concretion	−5.5	[*1*]
DDH-*222-45.45*	Moore	carbonaceous sedimentary rocks	pyrite concretion	−6.3	[*1*]
DDH-*222-85.85*	Moore	carbonaceous sedimentary rocks	pyrite concretion	−4.2	[*1*]
DDH-*242-70.45*	Moore	carbonaceous sedimentary rocks	pyrite bed	−2.7	[*1*]
DDH-*242-112*	Moore	carbonaceous sedimentary rocks	pyrite bed	−7.2	[*1*]
DDH-*112-15*	Moore	carbonaceous sedimentary rocks	pyrite bed	−3.8	[*2*]
DDH-*101-21*	Moore	carbonaceous sedimentary rocks	pyrite bed	−3.5	[*2*]
DDH-*100-16*	Moore	carbonaceous sedimentary rocks	pyrite bed	−8.0	[*2*]
Tunnel *2-#5*	Moore	carbonaceous sedimentary rocks	pyrite bed	−6.0	[*2*]
DDH-*240-95.5*	Moore	carbonaceous sedimentary rocks	pyrite framboid	<0.6	[*1*]
DDH-*240-102*	Moore	carbonaceous sedimentary rocks	pyrite framboid	−17.5	[*1*]
DDH-*242-70.45*	Moore	carbonaceous sedimentary rocks	pyrite framboid	+4.8	[*1*]
DDH-*242-196.5*	Moore	carbonaceous sedimentary rocks	pyrite framboid	−5.9	[*1*]
DDH-*233-41.5*	Moore	carbonaceous sedimentary rocks	pyrite framboid	+2.7	[*1*]
DDH-*222-85.85*	Moore	carbonaceous sedimentary rocks	pyrite framboid	+4.1	[*1*]
DDH-*240-23.5*	Moore	carbonaceous sedimentary rocks	pyrite cube	−3.8	[*1*]
DDH-*240-81.5*	Moore	carbonaceous sedimentary rocks	pyrite cube	−2.2	[*1*]
DDH-*240-89.5*	Moore	carbonaceous sedimentary rocks	pyrite cube	−5.0	[*1*]
DDH-*240-95.5*	Moore	carbonaceous sedimentary rocks	pyrite cube	0.0	[*1*]
DDH-*240-102*	Moore	carbonaceous sedimentary rocks	pyrite cube	−5.5	[*1*]
DDH-*242-112*	Moore	carbonaceous sedimentary rocks	pyrite cube	−5.2	[*1*]
DDH-*244-41.5*	Moore	carbonaceous sedimentary rocks	pyrite cube	−5.3	[*1*]
DDH-*233-72*	Moore	carbonaceous sedimentary rocks	pyrite cube	−5.6	[*1*]
DDH-*222-45.45*	Moore	carbonaceous sedimentary rocks	pyrite cube	−6.8	[*1*]
DDH-*191-143*	Moore	carbonaceous sedimentary rocks	pyrite cube	−5.8	[*1*]
DDH-*195-160*	Monte Negro	spilite	pyrite cube	−11.8	[*1*]
DDH-*196-140*	Monte Negro	spilite	pyrite cube	−7.8	[*1*]
DDH-*240-87*	Moore	carbonaceous sedimentary rocks	pyritohedral pyrite	−4.9	[*1*]
DDH-*240-95.5*	Moore	carbonaceous sedimentary rocks	pyritohedral pyrite	−6.0	[*1*]
DDH-*240-102*	Moore	carbonaceous sedimentary rocks	pyritohedral pyrite	−5.6	[*1*]
DDH-*242-112*	Moore	carbonaceous sedimentary rocks	pyritohedral pyrite	−5.0	[*1*]
DDH-*242-134.8*	Moore	carbonaceous sedimentary rocks	pyritohedral pyrite	−4.6	[*1*]
DDH-*242-196.5*	Moore	carbonaceous sedimentary rocks	pyritohedral pyrite	−3.9	[*1*]
DDH-*242-209.6*	Moore	carbonaceous sedimentary rocks	pyritohedral pyrite	−4.9	[*1*]
DDH-*233-41.5*	Moore	carbonaceous sedimentary rocks	pyritohedral pyrite	−3.6	[*1*]
DDH-*195-248*	Monte Negro	spilite	pyritohedral pyrite	−9.2	[*1*]
DDH-*240-70.9*	Moore	carbonaceous sedimentary rocks	vein pyrite	−7.0	[*1*]
DDH-*240-80.1*	Moore	carbonaceous sedimentary rocks	vein pyrite	−7.2	[*1*]
DDH-*240-80.1*	Moore	carbonaceous sedimentary rocks	vein pyrite	−7.9	[*1*]
DDH-*242-95*	Moore	carbonaceous sedimentary rocks	vein pyrite	−6.2	[*1*]
DDH-*242-98.5*	Moore	carbonaceous sedimentary rocks	vein pyrite	−5.9	[*1*]
DDH-*242-134.8*	Moore	carbonaceous sedimentary rocks	vein pyrite	−5.6	[*1*]

TABLE 4 *(continued)*

Specimen	Orebody	Lithology	Sample	$\delta^{34}S_{CDT}$ (‰)	Source*
DDH-*161-133*	Moore	carbonaceous sedimentary rocks	vein pyrite	−4.9	[*1*]
DDH-*159-176*	Moore	carbonaceous sedimentary rocks	vein pyrite	−5.0	[*1*]
DDH-*206-49*	Monte Negro	spilite	vein pyrite	−6.8	[*1*]
DDH-*177-205*	Moore	spilite	vein pyrite	−3.6	[*2*]
RD-*72-22*	Moore	carbonaceous sedimentary rocks	vein pyrite	−6.8	[*2*]
DDH-*195-246.9*	Monte Negro	spilite	vein pyrite	−9.5	[*3*]
DDH-*177-205*	Moore	spilite	vein alunite	+21.6	[*2*]
DDH-*195-246.9*	Monte Negro	spilite	vein alunite	+20.0	[*3*]
DDH-*92-46*	Moore	carbonaceous sedimentary rocks	vein barite	+18.8	[*2*]
DDH-*98-23*	Moore	carbonaceous sedimentary rocks	vein barite	+20.0	[*2*]

**Sources:* [*1*] = this study; [*2*] = Kesler et al. (1981); [*3*] = Muntean et al. (1990).

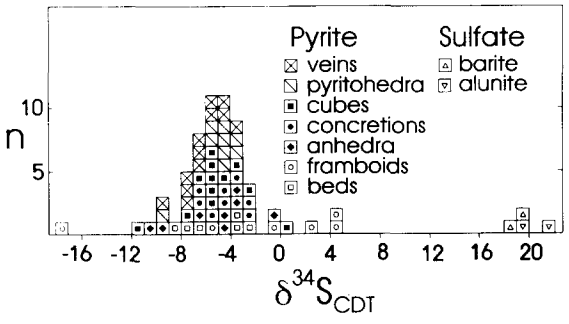

Fig. 12. Histogram of $\delta^{34}S$ data obtained from Pueblo Viejo pyrite and sulfates.

(3) Vein pyrite has $\delta^{34}S$-values that range from −9.5 to −3.6‰ and average −6.4‰, only slightly lighter than those observed for the NFDP.

(4) Alunite and barite from veins have $\delta^{34}S$-values that range from +18.8 to +21.6‰ (Kesler et al., 1981; Muntean et al., 1990).

The different morphologies of NFDP are indistinguishable isotopically from one another (Fig. 12). The $\delta^{34}S$-values of NFDP are similar to those of the vein pyrite and are indicative of a common source of sulfur. The $\delta^{34}S$ of NFDP range from −11.8 to 0.0‰ with 36 of the 43 values between −8 and −2‰. The NFDP with the lightest value shown in Fig. 12 was obtained from spilite and could not be the product of biogenic sulfate reduction. Although samples of NFDP from a single specimen have very similar $\delta^{34}S$-values, pyrite framboids from the same specimen will have quite different $\delta^{34}S$-values. Pyrite framboids in specimen DDH-240-102 have $\delta^{34}S$ of −17.5‰ while pyritohedral pyrite, pyrite concretions and pyrite cubes from the same specimen have $\delta^{34}S$-values of −5.6, −4.9 and −5.5‰, respectively (Table 4). The pyrite framboids containing the heaviest sulfur (+4.8‰, DDH-242-70.45) coexist with a layer of pyrite and anhedral pyrite that are depleted in ^{34}S (−2.7 and −3.4‰, respectively) (Table 4).

We interpret the similarity in the $\delta^{34}S$-values of the NFDP and vein pyrite to indicate a common source of sulfur. We conclude that this S had a magmatic–hydrothermal origin based on the relation between the $\delta^{34}S$-values obtained from sulfide to those obtained from sulfates. Muntean et al. (1990) have obtained $\delta^{34}S$-values of −9.5 and +20.0‰ from coeval pyrite and alunite, respectively (see Table 4) in the Monte Negro orebody. They have interpreted this pyrite–alunite pair to be in equilibrium and have calculated an equilibration temperature of 184°C. This temperature is in agreement with an estimate of 222°C from an alunite–pyrite intergrowth in the Moore orebody [data from Kesler et al. (1981), recalculated by Muntean et al. (1990)]. The pyrite–alunite pairs would have equilibrated in a fluid with a bulk $\delta^{34}S$-value near 0‰ under oxidizing conditions (as required by the presence of alunite). The $\delta^{34}S$-values of the NFDP reflect

the more reducing conditions (and higher sulfide/sulfate ratios) encountered in the carbonaceous sedimentary rocks. The pyrite–alunite systematics are similar to those observed at Summitville, Colorado, U.S.A. (Rye et al., 1990) and indicate a similar magmatic–hydrothermal origin (Rye et al., 1989).

The pyrite framboids probably formed during anoxic–sulfidic diagenesis, with the sulfide produced by biogenic reduction of maar-water sulfate. The wide range of δ^{34}S-values is consistent with bacterial sulfate reduction. We interpret the positive δ^{34}S-values, combined with the presence of abundant siderite distal to mineralization, as evidence that sulfate reduction occurred in a system closed to sulfate (Ohmoto and Rye, 1979; Berner, 1981; Ohmoto, 1986) and that pyrite formation during early diagenesis was limited by the availability of S rather than Fe or reactive organic matter. There are two potential sources of the maar-water sulfate: (1) sulfate derived from weathering of sulfides and sulfates (normal runoff); and (2) sulfate derived from the magmatic–hydrothermal system. Sulfate that escaped to the maar-waters would have been +10 to +20‰ while any H_2S that was oxidized in the maar would have had δ^{34}S-values of −10 to 0‰; thus, only the sulfate derived from the magmatic–hydrothermal system could produce the values observed.

Each of the two types of disseminated pyrite in the carbonaceous sedimentary rocks had a unique origin even though they may have derived their sulfur from the same igneous source. The framboidal pyrite formed during biogenic sulfate reduction. Siderite formed during methanogenesis, after all sulfate had been depleted. The NFDP formed when an H_2S-rich hydrothermal fluid reacted with the siderite in the sedimentary rocks to form pyrite.

8. Significance of sulfidation to mineralization

The significance of the sulfidation of ferrous Fe to disseminated mineralization can be discussed by considering a phase diagram for the Fe–C–O–S system in log f_{O_2}–log a_{H_2S} space (Fig. 13). The composition of the fluids that produced the disseminated mineralization is shown by the black dot in Fig. 13. This black dot represents the composition of the hydrothermal fluid while in equilibrium with the assemblage quartz–alunite–pyrite that has been described in the core of the Moore and Monte Negro systems (Kesler et al., 1981; Muntean et al., 1990). When this fluid came into contact with siderite both oxidants and S were consumed, the fluid moved toward equilibrium with siderite, and crossed the Au solubility contours shown in Fig. 13 at a high angle. The reaction for sulfidation of siderite in log f_{O_2}–log a_{H_2S} space is:

$$FeCO_3 + 2H_2S + \tfrac{1}{2}O_2 \rightleftharpoons FeS_2 + CO_2 + 2H_2O \quad (2)$$

which has a slope of −4 in log f_{O_2}–log a_{H_2S} space, while the reaction for Au deposition:

$$\tfrac{1}{2}H_2O + Au(HS)_2^- + H^+ \rightleftharpoons 2H_2S + Au + \tfrac{1}{4}O_2 \quad (3)$$

has a slope of 8 in log f_{O_2}–log a_{H_2S} space. Adding these two reactions yields the combined reaction controlling Au deposition:

$$FeCO_3 + \tfrac{1}{4}O_2 + Au(HS)_2^- + H^+ \rightleftharpoons FeS_2 + CO_2 + \tfrac{3}{2}H_2O + Au \quad (4)$$

The stability field of siderite will be increased if a_{FeCO_3} declines or if the f_{CO_2} is increased. To test the sensitivity of Au deposition to variations in these two parameters the siderite stability field was redrawn reflecting the composition of the siderite at Pueblo Viejo ($X_{FeCO_3} \geq 0.7$ and assuming ideal mixing) and increasing f_{CO_2} to 10 bar (Fig. 13). Sulfidation of siderite remains a powerful mechanism for Au deposition, even with these changes. This mechanism is also robust to possible errors in

TABLE 5

Equilibrium constants used to construct Fig. 13

Reaction	log K_{473K}	Source*
$H_2S_{(aq)} + 2O_2 \rightleftharpoons HSO_4^- + H^+$	71.3	[1], [2]
$H_2S_{(aq)} \rightleftharpoons H^+ + HS^-$	−6.9	[2]
$2H_2S_{(aq)} + O_2 \rightleftharpoons 2S_{(l)} + 2H_2O$	41.0	[1], [2], [3]
$4FeS_2 + 15O_2 + 8H_2O \rightleftharpoons 2Fe_2O_3 + 8H^+ + 8HSO_4^-$	494.20	[1], [2]
$FeS + H^+ + HS^- \rightleftharpoons FeS_2 + H_2$	9.81	[1]
$4Fe_3O_4 + O_2 \rightleftharpoons 6Fe_2O_3$	40.49	[1]
$3FeCO_3 + \frac{1}{2}O_2 \rightleftharpoons Fe_3O_4 + 3CO_2$	24.76	[1]
$Au + H_2S_{(aq)} + HS^- + \frac{1}{4}O_2 \rightleftharpoons Au(HS)_2^- + \frac{1}{2}H_2O$	9.70	[1], [2], [4]
$Au + H^+ + 2Cl^- + \frac{1}{4}O_2 \rightleftharpoons AuCl_2^- + \frac{1}{2}H_2O$	2.23	[2]
$H_2 + \frac{1}{2}O_2 \rightleftharpoons H_2O$	23.18	[1]

*Sources: [1] = SUPCRT (see Bowers et al., 1984; Helgeson et al., 1978); [2] = Helgeson (1969); [3] = Barton and Skinner (1979); [4] = Shenberger and Barnes (1989).

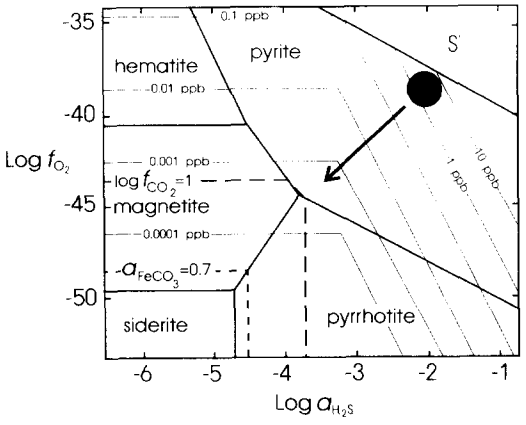

Fig. 13. Plot of the Fe–C–O–S system in log f_{O_2}–log a_{H_2S} space. Equilibrium constants used to construct this diagram are given in Table 5. Diagram drawn for $T = 200°C$, pH = 2.5, $I = 1$ *m* NaCl, and $f_{CO_2} = 1$ bar. The *dashed lines* show the siderite stability field for $a_{FeCO_3} = 0.7$ and $f_{CO_2} = 10$ bar. The *contour lines* indicate the solubility of Au in ppb; where these *contours* are horizontal Au is complexed by Cl^-, predominantly, Au-bisulfide predominates where the *contours* slope.

determining the intial fluid composition. Changing a_{H_2S} by an order of magnitude or f_{O_2} by more than 5 orders of magnitude will not change the relations shown in Fig. 13 significantly.

Although the arrow shown in Fig. 13 illustrates the mechanism of Au deposition, it is not meant to depict the evolution of the fluid–rock system in detail. A more detailed description of the chemistry of sulfidation of ferrous Fe and its importance for Au deposition has been presented by Böhlke (1988). Muntean (1989) examined the relative importance of sulfidation versus other potential Au deposition mechanisms. By modelling the Pueblo Viejo system using the CHILLER and SOLVEQ computer programs (Reed, 1982; Reed and Spycher, 1985; Spycher and Reed, 1988). Muntean (1989) was able to compare the efficiency of Au deposition by sulfidation against fluid mixing and boiling. While all three mechanisms were capable of depositing significant amounts of Au, only sulfidation yielded gangue assemblages consistent with those observed at Pueblo Viejo. Added to the modelling results, the observations in this paper suggest that sulfidation is the most likely mechanism for producing the disseminated mineralization.

9. Importance of Fe–C–S diagenesis to Au mineralization

The mineralogic products of biogenic sulfate reduction and methanogenesis in the maar sediments exerted first-order controls on later disseminated Au mineralization. The sulfate-depleted, reducing, lacustrine environment present during diagenesis led to the fixing of

reduced Fe in siderite. The capacity of the rock to consume H_2S, destroy the $Au(HS)_2^-$ complex and deposit Au was controlled by the amount of non-pyrite Fe in the rock. Carbonaceous sedimentary rocks from DDH-223 (Fig. 2) in which NFDP is absent contained 8% Fe and have DOS-values of 0.19. Each kilogram of this rock could have consumed 2.3 mol H_2S. On the other hand, pyrite comprises as much as 80% of the Fe in sediments where pyrite deposition was limited by the availability of Fe (Raiswell and Berner, 1985; Raiswell et al., 1988). Each kilogram of such a rock could have consumed only 0.57 mol H_2S (assuming Fe content of 8%). Although organic matter was also a sink for hydrothermal S and could have exerted a control on Au deposition (Kettler et al., 1990) the greater abundance of Fe made it a more important sink for H_2S.

10. Conclusions

Disseminated mineralization at Pueblo Viejo comprises pyrite, Au, gratonite, calaverite and enargite. Disseminated pyrite has two different origins:

(1) Pyrite framboids in the carbonaceous sedimentary rocks were formed by biogenic reduction of sulfate in a maar environment. Biogenic sulfate reduction occurred in a closed system with the availability of sulfate limiting the conversion of Fe to pyrite. After sulfate was exhausted, siderite formed in the ensuing anoxic–methanic environment.

(2) Non-framboid disseminated pyrite formed during mineralization when a hydrothermal fluid encountered the abundant ferrous Fe that was present as siderite in the carbonaceous sedimentary rocks of the Pueblo Viejo Member. The ferrous Fe was sulfidized to form pyrite, a process that effected Au mineralization by reducing the fluid and consuming H_2S. If the formation of diagenetic pyrite had not been limited by the availability of sulfate in the pore waters, Fe^{2+} would have been sequestered as pyrite during diagenesis. If the Fe^{2+} had been sequestered as pyrite the capacity of the rocks to consume H_2S in the later hydrothermal fluids would have been diminished greatly.

Acknowledgments

This paper formed a part of the senior author's dissertation at the University of Michigan. The authors would like to thank M. Seaward and M. Bath for field, logistical and analytical support at Pueblo Viejo. They have also provided valuable interpretations and insight. M. Wasserman, J. Deen, C. Jung, D. Dettman and K.C. Lohmann assisted in obtaining the stable isotope data. C.H. Henderson assisted us in collecting data with the microprobe and SEM. Discussions with W.C. Kelly, R.E. Beane, C.N. Alpers, E.L. Shock, G. Faure, M.L. Tuttle and E.J. Essene, and reviews of this manuscript by J.L. Muntean, J.C.G. Walker, J.E. Penner-Hahn, J.S. Leventhal, J.K. Böhlke, K.C. Lohmann and R.R. Seal II are greatly appreciated. Careful reviews for this journal by T.F. Anderson and an anonymous referee, and for the U.S. Geological Survey by A.H. Hofstra and R.I. Grauch have improved the manuscript. None of the aforementioned necessarily agrees with the conclusions. The electron microprobe and SEM used in this work were provided by National Science Foundation grants BSR-83-14092 and EAR-82-12764. Research at Pueblo Viejo has been supported by Rosario Dominicana S.A. and National Science Foundation grant EAR-8607021 to S.E.K. and P.A.M.

References

Barton, Jr., P.B. and Skinner, B.F., 1979. Sulfide mineral stabilities. In: H.L. Barnes (Editor), Geochemistry of Hydrothermal Ore Deposits. Wiley, New York, N.Y., pp. 278–403.

Bernard, A. and Symonds, R.B., 1989. The significance of siderite in the sediments from Lake Nyos, Cameroon. J. Volcanol. Geotherm. Res., 42: 187–194.

Berner, R.A., 1981. A new geochemical classification of

sedimentary environments. J. Sediment. Petrol., 51: 359–365.

Boesen, C. and Postma, D., 1988. Pyrite formation in anoxic sediments of the Baltic. Am. J. Sci., 288: 575–603.

Böhlke, J.K., 1988. Carbonate–sulfide equilibria and "stratabound" disseminated epigenetic gold mineralization: a proposal based on examples from Alleghany, California, U.S.A. Appl. Geochem., 3: 499–516.

Bowers, T.S., Jackson, K.J. and Helgeson, H.C., 1984. Equilibrium activity diagrams for coexisting minerals and aqueous solutions at pressures to 5 kb and 600°C. Springer, Berlin, 397 pp.

Bowin, C.O., 1975. The geology of Hispaniola. In: A.E.M. Nairn and F.G. Stehli (Editors), The Ocean Basins and Margins. Plenum, New York, N.Y., pp. 501–552.

Carpenter, S.J., Erickson, J.M., Lohmann, K.C. and Owen, M.R., 1988. Diagenesis of fossiliferous concretions from the Upper Cretaceous Fox Hills Formation, North Dakota. J. Sediment. Petrol., 58: 706–723.

Carothers, W.W., Adami, L.H. and Rosenbauer, R.J., 1988. Experimental oxygen isotope fractionation between siderite–water and phosphoric acid liberated CO_2–siderite. Geochim. Cosmochim. Acta, 52: 2445–2450.

Craig, H., 1957. Isotopic standards for carbon and oxygen correction factors for mass spectrometric analysis of carbon dioxide. Geochim. Cosmochim. Acta, 12: 133–149.

Curtis, C.D., Coleman, M.L. and Love, L.G., 1986. Pore water evolution during sediment burial from isotopic and mineral chemistry of calcite, dolomite and siderite concretions. Geochim. Cosmochim. Acta, 50: 2321–2334.

Drummond, S.E. and Ohmoto, H.L., 1985. Chemical evolution and mineral deposition in boiling hydrothermal systems. Econ. Geol., 80: 126–147.

Fritz, P., Binda, P.L., Folinsbee, F.E. and Krouse, H.R., 1971. Isotopic composition of diagenetic siderites from Cretaceous sediments, western Canada. J. Sediment. Petrol., 41: 282–288.

Gautier, D.L., 1982. Siderite concretions: Indicators of early diagenesis in the Gammon Shale (Cretaceous). J. Sediment. Petrol., 52: 859–871.

Giggenbach, W.F., 1990. Water and gas chemistry of Lake Nyos and its bearing on the eruptive process. J. Volcanol. Geotherm. Res., 42: 337–362.

Hartley, J.N. and Wick, O.J., 1979. Mineralogical investigation of five selected samples from the Pueblo Viejo sulfide ore. Batelle Pac. Northw. Lab., Richland, Wash., private report for Rosario Dominicana, S.A., Santo Domingo.

Helgeson, H.C., 1969. Thermodynamics of hydrothermal systems at elevated temperatures and pressures. Am. J. Sci., 267: 729–804.

Helgeson, H.C., Delaney, J.C., Nesbitt, H.W. and Bird, D.K., 1978. Summary and critique of the thermodynamic properties of rock-forming minerals. Am. J. Sci., 278-A: 1–299.

Hoefs, J., 1980. Stable Isotope Geochemistry. Springer, 2nd ed., Berlin, 208 pp.

Hofstra, A.H., Northrop, H.R., Rye, R.O., Landis, G.P. and Birak, D.J., 1998. Origin of sediment-hosted disseminated gold deposits by fluid mixing: evidence from jasperoids in the Jerritt Canyon gold district, Nevada, USA. Bicent. Gold 88, Extend. Abstr. Prog., Geol. Soc. Aust. Abstr., Ser. No. 22, pp. 284–289.

Hofstra, A.H., Leventhal, J.S., Northrop, H.R., Landis, G.P., Rye, R.O., Birak, D.J. and Dahl, A.R., 1991. Genesis of sediment-hosted gold deposits by fluid mixing and sulfidization: Chemical reaction path modeling of ore-depositional processes documented in the Jerritt Canyon District, Nevada. Geology, 19: 36–40.

Irwin, H., Coleman, M.L. and Curtis, C.D., 1977. Isotopic evidence for the source of diagenetic carbonates formed during burial of organic rich sediments. Nature (London), 269: 209–213.

Kelly, W.C. and Turneare, F.S., 1970. Mineralogy, paragenesis and geothermometry of tin and tungsten deposits of the eastern Andes, Bolivia. Econ. Geol., 65: 609–680.

Kesler, S.E., Russell, N., Seaward, M., Rivera, J., McCurdy, K., Cumming, G.L. and Sutter, J.F., 1981. Geology and geochemistry of sulfide mineralization underlying the Pueblo Viejo gold–silver oxide deposit, Dominican Republic. Econ. Geol., 76: 1096–1117.

Kesler, S.E., Kettler, R.M., Meyers, P.A., Dunham, K.W., Russell, N., Seaward, M. and McCurdy, K., 1986. Relation between organic material and precious metal mineralization in the Moore orebody, Pueblo Viejo, Dominican Republic. In: W.E. Dean (Editor), Organics and Ore Deposits: Proceedings of the Denver Region Exploration Geologists Society Symposium, Denver Reg. Explor. Geol. Soc., Denver, Colo., pp. 105–110.

Kesler, S.E., Russell, N., Polanco, J., McCurdy, K. and Cumming, G.L., 1991. Geology and geochemistry of the Early Cretaceous Los Ranchos Formation, Central Dominican Republic. In: P. Mann, G. Draper and J.F. Lewis (Editors), Geologic and Tectonic Development of the North American–Caribbean Plate Boundary in Hispaniola. Geol. Soc. Am., Spec. Pap., 262: 187–202.

Kettler, R.M., Kesler, S.E., Meyers, P.A., Russell, N. and Polanco, J., 1987. Precious metal mineralization by sulfidation of ferrous iron and organic matter in the Moore gold–silver deposit, Pueblo Viejo, Dominican Republic. Geol. Soc. Am., Abstr. Prog., 19: 726.

Kettler, R.M., Waldo, G.S., Penner-Hahn, J.E., Meyers, P.A. and Kesler, S.E., 1990. Sulfidation of organic matter associated with gold mineralization, Moore orebody, Pueblo Viejo, Dominican Republic. Appl. Geochem., 5: 237–248.

Leventhal, J.S., 1983. An interpretation of carbon and

sulfur relationships in Black Sea sediments as indicators of environments of deposition. Geochim. Cosmochim. Acta, 47: 133–137.

Matsumoto, R. and Ijima, A., 1981. Origin and diagenetic evolution of Ca,Mg,Fe carbonates in some coalfields of Japan. Sedimentology, 28: 239–259.

Maynard, J.B., 1982. Extension of Berner's "New geochemical classification of sedimentary environments" to ancient sediments. J. Sediment. Petrol., 52: 1325–1331.

Middelburg, J.J., 1991. Organic carbon, sulphur and iron in recent semi-euxinic sediments of Kau Bay, Indonesia. Geochim. Cosmochim. Acta, 55: 815–828.

Mozley, P.S., 1989. Relation between depositional environment and the elemental composition of early diagenetic siderite. Geology, 17: 704–706.

Muntean, J.L., 1989. Evolution of the Monte Negro acid–sulfate Au–Ag deposit Pueblo Viejo, Dominican Republic: Important factors in grade development. M.S. Thesis, University of Michigan, Ann Arbor, Mich., 61 pp.

Muntean, J.L., Kesler, S.E., Russell, N. and Polanco, J., 1990. Evolution of the Monte Negro acid–sulfate Au–Ag deposit Pueblo Viejo, Dominican Republic: Important factors in grade development. Econ. Geol., 85: 1738–1758.

Murowchick, J.B. and Barnes, H.L., 1987. Effects of temperature and degree of supersaturation on pyrite morphology. Am. Mineral., 72: 1241–1250.

Norman, D.I., 1987. Why some geothermal systems deposit Au–Ag ores. Geol. Soc. Am., Abstr. Prog., 19: 790.

Ohmoto, H.L., 1986. Stable isotope geochemistry of ore deposits. Am. Soc. Mineral., Rev. Mineral., 16: 491–559.

Ohmoto, H.L. and Rye, R.O., 1979. Isotopes of sulfur and carbon. In: H.L. Barnes (Editor), Geochemistry of Hydrothermal Ore Deposits. Wiley, New York, N.Y., pp. 509–567.

Phillips, G.N. and Groves, D.I., 1983, Fluid access and fluid–wallrock interaction in the genesis of the Archaean gold–quartz vein deposit at Hunt mine, Kambalda, Western Australia. In: R.P. Foster (Editor), Gold '82 — Proceedings of the International Symposium, Zimbabwe. A.A. Balkema, Rotterdam, pp. 389–416.

Phillips, G.N., Groves, D.I. and Martyn J.E., 1984. An epigenetic origin for Archean banded iron-formation-hosted gold deposits. Econ. Geol., 79: 162–171.

Raiswell, R. and Berner, R.A., 1985. Pyrite formation in euxinic and semi-euxinic sediments. Am. J. Sci., 285: 710–724.

Raiswell, R., Buckley, F., Berner, R.A. and Anderson, T.F., 1988. Degree of pyritization of iron as a paleoenvironmental indicator of bottom water oxygenation. J. Sediment. Petrol., 58: 812–819.

Ramdohr, P., 1980. The Ore Minerals and Their Intergrowths. Pergamon, London, 1205 pp.

Reed, M.H., 1982. Calculation of multicomponent chemical equilibria and reaction processes in systems involving minerals, gases, and an aqueous phase. Geochim. Cosmochim. Acta, 46: 513–528.

Reed, M.H. and Spycher, N., 1985. Boiling, cooling, and oxidation in epithermal systems: A numerical modeling approach. Rev. Econ. Geol., 2: 249–272.

Rosenbaum, R.J. and Sheppard, S.M.F., 1986. An isotopic study of siderites, dolomites and ankerites at high temperatures. Geochim. Cosmochim. Acta, 50: 1147–1150.

Russell, N. and Kesler, S.E., 1991. Geology of the maar–diatreme complex hosting precious metal mineralization at Pueblo Viejo, Dominican Republic. In: P. Mann, G. Draper and J.F. Lewis (Editors), Geologic and Tectonic Development of the North American–Caribbean Plate Boundary in Hispaniola. Geol. Soc. Am., Spec. Pap., 262: 203–216.

Russell, N., Seaward, M., Rivera, J.A., McCurdy, K., Kesler, S.E. and Cloke, P.L., 1981. Geology and geochemistry of the Pueblo Viejo gold–silver oxide ore deposit. Inst. Min. Metall. Trans., Sect. B, 90: B153–B162.

Russell, N., Polanco, J. and Kesler, S.E., 1986. Geology of the Monte Negro gold–silver deposit, Pueblo Viejo district, Dominican Republic. In: A.J. Macdonald (Editor), Proceedings of Gold '86, International Symposium on the Geology of Gold. GOLD '86, Toronto, Ont., pp. 497–503.

Rye, R.O., Roberts, R.J., Snyder, W.S., Lahusen, G.L. and Motica, J.E., 1984. Textural and stable isotope studies of the Big Mike cupriferous volcanogenic massive sulfide deposit, Pershing County, Nevada. Econ. Geol., 79: 124–140.

Rye, R.O., Bethke, P.M. and Wasserman, M.D., 1989. Diverse origins of alunite and acid–sulfate alteration: stable isotope systematics. U.S. Geol. Surv., Open-File Rep. 89-5, 20 pp.

Rye, R.O., Stoffregen, R. and Bethke, P.M., 1990. Stable isotope systematics and magmatic and hydrothermal processes in the Summitville, CO gold deposit. U.S. Geol. Surv., Open-File Rep. 90-626, 31 pp.

Schoonen, M.A.A. and Barnes, H.L., 1988. Kinetics of hydrothermal pyrite and marcasite formation from solution. Geol. Soc. Am., Abstr. Prog., 20: A43.

Seward, T.M., 1973. Thio complexes of gold in hydrothermal ore solutions. Geochim. Cosmochim. Acta, 37: 379–399.

Shenberger, D.M. and Barnes, H.L., 1989. Gold solubility in aqueous sulfide solutions from 150 to 350°C. Geochim. Cosmochim. Acta, 53: 269–278.

Sillitoe, R.H. and Bonham, Jr., H.F., 1984. Volcanic landforms and ore deposits. Econ. Geol., 79: 1286–1298.

Spycher, N.F. and Reed, M.H., 1988. Fugacity coefficients of H_2, CO_2, CH_4, H_2O and of H_2O–CO_2–CH_4 mixtures: A virial equation treatment for moderate pressures applicable to calculations of hydrothermal boiling. Geochim. Cosmochim. Acta, 52: 739–749.

Walters, L.J., Claypool, G.E. and Choquette, P.W., 1972.

Reaction rates and $\delta^{18}O$ variation for the carbonate–phosphoric acid preparation method. Geochim. Cosmochim. Acta, 36: 129–140.

Wood, S.A., Crerar, D.A. and Borcsik, M.P., 1987. Solubility of the assemblage pyrite–pyrrhotite–magnetite–sphalerite–galena–gold–stibnite–bismuthinite–argentite–molybdenite in H_2O–NaCl–CO_2 solutions from 200 to 350°C. Econ. Geol., 81: 1864–1887.